MITSUBISHI ELECTRIC RESEARCH LABORATORIES
https://www.merl.com

Reconfigurable Intelligent Surface-Assisted Spatial Scattering Modulation

Zhu, Xusheng; Yuan, Lei; Kim, Kyeong Jin; Li, Qingqing; Zhang, Jiliang

TR2022-008 January 27, 2022

Abstract

Reconfigurable intelligent surface (RIS) and spatial scattering modulation (SSM) are promising candidates for future generations of wireless communication. The former provides an enhanced transmission environment by providing an alternative communication path, while the latter boosts the spectral efficiency. In this letter, we firstly propose a novel uplink millimeterwave(mmWave) communication system that utilizes both RIS and SSM to support data transmission over wireless channels. We design the reflecting phase shifters at the RIS to maximize the signal-to-noise ratio of the two-hop communications. Moreover, a maximum likelihood detector is adopted to a new system with RIS-SSM and a new closed-form expression for a tight union upper bound on the bit error rate (BER) is derived. Monte Carlo simulation results are provided to verify the accuracy of the derived analytical expression. Numerical results reveal that the proposed RIS-SSM scheme has a significantly lower BER than the traditional SSM.

IEEE Communications Letters 2022

Mitsubishi Electric Research Laboratories, Inc.
201 Broadway, Cambridge, Massachusetts 02139

Reconfigurable Intelligent Surface-Assisted Spatial Scattering Modulation

Xusheng Zhu, Lei Yuan, *Member, IEEE*, Kyeong Jin Kim, *Senior Member, IEEE*, Qingqing Li, Jiliang Zhang, *Senior Member, IEEE*

***Abstract*—Reconfigurable intelligent surface (RIS) and spatial scattering modulation (SSM) are promising candidates for future generations of wireless communication. The former provides an enhanced transmission environment by providing an alternative communication path, while the latter boosts the spectral efficiency. In this letter, we firstly propose a novel uplink millimeter-wave (mmWave) communication system that utilizes both RIS and SSM to support data transmission over wireless channels. We design the reflecting phase shifters at the RIS to maximize the signal-to-noise ratio of the two-hop communications. Moreover, a maximum likelihood detector is adopted to a new system with RIS-SSM and a new closed-form expression for a tight union upper bound on the bit error rate (BER) is derived. Monte Carlo simulation results are provided to verify the accuracy of the derived analytical expression. Numerical results reveal that the proposed RIS-SSM scheme has a significantly lower BER than the traditional SSM.**

***Index Terms*—Reconfigurable intelligent surface, spatial scattering modulation, maximum likelihood detection, average bit error probability.**

I. Introduction

With the commercialization of fifth-generation (5G) communication networks, technologies for sixth-generation (6G) communications are being explored to realize faster and more reliable data transmission [1]. A disruptive 6G wireless system is designed to be inherently suited to the performance of Internet of Everything (IoE) applications requirements and the accompanying technology trends [2]. Among the technical works related to 6G, the RIS is one of the most eye-catching protagonists, which is considered as a paradigm shift and a revolutionary wireless communication technology [3].

Extensive research efforts on RIS have been conducted to investigate in the state-of-the-art literature. A survey on the RIS has demonstrated that the use of RIS has emerged as a promising technology for future wireless communication networks [4]. Moreover, the RIS consisting of a large amount of low-cost passive units can reflect the incident signal independently by altering wavefront, e.g., the phase, amplitude, frequency, and even polarization [5]. Hence, three-dimensional (3D) passive beamforming can be directly realized without a transmit radio frequency (RF) chain. In other words, RIS can effectively reduce the energy consumption of the wireless communication system, compared with massive multiple-input multiple-output (MIMO) for millimeter-wave (mmWave) beamforming [6], [7]. It should be noted that the authors of [8] discussed the similarities and differences between relays and RISs. In addition, the authors of [9] addressed the theoretical performance limits of RIS-assisted communication systems, and illustrated potential use cases of RIS in wireless networks.

Spatial scattering modulation (SSM), which activates a single scatterer per transmission and exploits the index of the active scatterer to carry extra bits of information, thereby significantly improving the spectral efficiency (SE) of the communication system [10]. In view of this, [11] and [12] presented adaptive SSM and generalized SSM schemes, respectively. Moreover, the asymptotic bit error rate (BER) in the high signal-to-noise ratio (SNR) region and the diversity gain of the SSM, were derived in [13]. Furthermore, the authors in [14] presented the polarized SSM scheme that improves the SE by increasing the degree of freedom in the polarization domain.

Recently, the concept of index modulation (IM) and its variants and applications to RIS-assisted systems, such as RIS-spatial modulation (RIS-SM) are investigated in [15]–[17]. To the best of our knowledge, the research on the SSM-assisted RIS system is still missing in the existing literature. Motivated by the aforementioned studies, a novel RIS-SSM scheme is proposed to make it possible ultra-reliable wireless communication systems. The main contributions of this letter are summarized as follows:

- We propose a RIS-based SSM scheme that provides not only ultra-reliable transmissions but also avoids interference problems by using scatterer indices.
- A set of optimal phase shifts is designed at the RIS. Moreover, the analytical expression for an upper bound on the BER is derived based on the conditional pairwise error probability (CPEP) and validated by link level simulations.
- Link level simulation results demonstrate that the proposed scheme provides better performance than the conventional SSM in terms of reliability.

II. System Model

A. Channel Model

In this section, we represent a RIS-SSM scheme for uplink mmWave system that the transmitter (Tx) and receiver (Rx) are respectively equipped with N_{t} and N_{r} antenna elements,

X. Zhu, L. Yuan, and Q. Li are with the School of Information Science and Engineering, Lanzhou University, Lanzhou, 730000, Gansu, China. (*Corresponding author: Lei Yuan.* (e-mail: yuanl@lzu.edu.cn).

K. J. Kim is with Mitsubishi Electric Research Laboratories (MERL), Cambridge, MA 02139 USA.

J. Zhang is with Department of Electronic and Electrical Engineering, the University of Sheffield, Sheffield, S1 4ET, U.K.

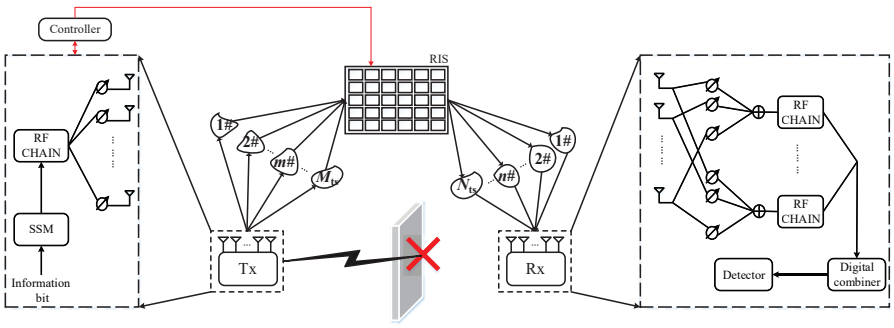

Fig. 1. RIS-assisted SSM system model for uplink transmissions.

and the RIS array with L reflecting elements as shown in Fig. 1. We assumed that there is no direct link between the Tx and Rx. The equivalent channel between them can be written as

$$\mathbf{H} = \mathbf{F}\boldsymbol{\Theta}\mathbf{G}, \tag{1}$$

where $\boldsymbol{\Theta} = \mathrm{diag}\left(\beta_1 e^{-j\phi_1}, \cdots, \beta_l e^{-j\phi_l}, \cdots, \beta_L e^{-j\phi_L}\right)$ denotes a diagonal matrix, where $\phi_l \in [0, 2\pi)$ and $\beta_l \in [0, 1]$ respectively denote the phase shift and the amplitude reflection coefficient of the lth element of the RIS [4]. To characterize the performance limit of RIS-SSM passive beamforming, we assume that $|\beta_l| = 1$ [19]. In addition, $\mathbf{G}$ is the channel matrix between the Tx and RIS via a scatterer [10]. Similarly, $\mathbf{F}$ denotes the channel matrix between the RIS and Rx via a scatterer. These channel matrices are respectively expressed as follows:

$$\begin{aligned}\mathbf{F} &= \sum\nolimits_{n=1}^{N_{ts}} h_n \boldsymbol{a}_{\mathrm{r}}\left(\theta_n\right) \boldsymbol{a}_{\mathrm{r,i}}^{\mathrm{H}}\left(\varphi_n, \vartheta_n\right), \\ \mathbf{G} &= \sum\nolimits_{m=1}^{M_{ts}} g_m \boldsymbol{a}_{\mathrm{i,t}}\left(\varphi_m, \vartheta_m\right) \boldsymbol{a}_{\mathrm{t}}^{\mathrm{H}}\left(\theta_m\right),\end{aligned} \tag{2}$$

where M_{ts} and N_{ts} respectively represent the number of scatterers from the Tx to RIS and from the RIS to Rx; g_m and h_n are the complex gains of the m-th and n-th paths. $(\cdot)^{\mathrm{H}}$ represents the Hermitian of a vector or a matrix. Each path complex gain is assumed to follow $\mathcal{CN}(0, 1)$ distribution under the assumption of flat Rayleigh fading channels [10]. In the sequel, $\mathcal{CN}(m, \sigma_n^2)$ denotes a circularly symmetric complex Gaussian random variable with mean m and variance σ_n^2. Based on uniform line array (ULA), the steering vectors $\boldsymbol{a}_r\left(\theta_n\right)$ at the Rx and $\boldsymbol{a}_t\left(\theta_m\right)$ at the Tx are respectively given as [10]

$$\begin{aligned}\boldsymbol{a}_{\mathrm{r}}(\theta_n) &= \frac{1}{\sqrt{N_{\mathrm{r}}}}[1, e^{j2\pi\psi_n}, \cdots, e^{j2\pi\psi_n \cdot n_{\mathrm{r}}}, \cdots, e^{j2\pi\psi_n \cdot (N_{\mathrm{r}}-1)}]^{\mathrm{T}}, \\ \boldsymbol{a}_{\mathrm{t}}(\theta_m) &= \frac{1}{\sqrt{N_{\mathrm{t}}}}[1, e^{j2\pi\psi_m}, \cdots, e^{j2\pi\psi_m \cdot n_{\mathrm{r}}}, \cdots, e^{j2\pi\psi_m \cdot (N_{\mathrm{t}}-1)}]^{\mathrm{T}},\end{aligned} \tag{3}$$

where $\psi_n = \frac{d_{\mathrm{r}}}{\lambda}\sin\left(\theta_n\right)$ and $\psi_m = \frac{d_{\mathrm{t}}}{\lambda}\sin\left(\theta_m\right)$. d_r and d_t denote antenna separation at the Rx and Tx, respectively. λ presents the carrier wavelength. $\theta_n \in [0, \pi)$ and $\theta_m \in [0, \pi)$ are the angle of arrival (AoA) and the angle of departure (AoD) of the n-th and m-th scatterers, respectively.

A uniform planar array (UPA) for the MIMO system is considered at the RIS in a 3D space, where a local coordinate system is defined with $\varphi \in [0, \pi)$ being the azimuth angle and $\vartheta \in [0, \pi)$ being the elevation angle. $\boldsymbol{a}_{\mathrm{r,i}}\left(\varphi_n, \vartheta_n\right)$ and $\boldsymbol{a}_{\mathrm{i,t}}\left(\varphi_m, \vartheta_m\right)$ denotes the AoAs from the Tx to RIS and the AoDs from the RIS to Rx, respectively, which can be described as [7]

$$\begin{aligned}\boldsymbol{a}_{\mathrm{r,i}}\left(\varphi_n, \vartheta_n\right) &= \sum\nolimits_{l=1}^{L} \mathbf{v}_{\mathrm{x}}\left(\varphi_{n,l}, \vartheta_{n,l}\right) \otimes \mathbf{v}_{\mathrm{y}}\left(\varphi_{n,l}, \vartheta_{n,l}\right), \\ \boldsymbol{a}_{\mathrm{i,t}}\left(\varphi_m, \vartheta_m\right) &= \sum\nolimits_{l=1}^{L} \mathbf{v}_{\mathrm{x}}\left(\varphi_{m,l}, \vartheta_{m,l}\right) \otimes \mathbf{v}_{\mathrm{y}}\left(\varphi_{m,l}, \vartheta_{m,l}\right),\end{aligned} \tag{4}$$

where $\otimes$ denotes the Kronecker product. The horizontal and vertical direction vectors present $\mathbf{v}_{\mathrm{x}}(\varphi, \vartheta)$ and $\mathbf{v}_{\mathrm{y}}(\varphi, \vartheta)$, respectively, which can be expressed as

$$\begin{aligned}\mathbf{v}_{\mathrm{x}}(\varphi,\vartheta) =& [1, e^{j(2\pi/\lambda)d_{\mathrm{x}}\sin(\varphi)\cos(\vartheta)}, \ldots, e^{j(2\pi/\lambda)d_{\mathrm{x}}\sin(\varphi)\cos(\vartheta)l_{\mathrm{x}}}, \\ & \ldots, e^{j(2\pi/\lambda)d_{\mathrm{x}}\sin(\varphi)\cos(\vartheta)(L_{\mathrm{x}}-1)}]^{\mathrm{T}}, \\ \mathbf{v}_{\mathrm{y}}(\varphi,\vartheta) =& [1, e^{j(2\pi/\lambda)d_{\mathrm{y}}\sin(\varphi)\cos(\vartheta)}, \ldots, e^{j(2\pi/\lambda)d_{\mathrm{y}}\sin(\varphi)\cos(\vartheta)l_{\mathrm{y}}}, \\ & \ldots, e^{j(2\pi/\lambda)d_{\mathrm{y}}\sin(\varphi)\cos(\vartheta)(L_{\mathrm{y}}-1)}]^{\mathrm{T}},\end{aligned} \tag{5}$$

where d_{x} and d_{y} denote the element intervals of the RIS row and column, respectively. Let $L = L_{\mathrm{x}} \times L_{\mathrm{y}}$, where L_{x} and L_{y} respectively denote the number of RIS elements on rows and columns. $l_{\mathrm{x}} = \mathrm{mod}\left(l-1, L_{\mathrm{x}}\right)$ and $l_{\mathrm{y}} = \lfloor (l-1)/L_{\mathrm{y}} \rfloor$ are the horizontal and vertical indices of element n, respectively. Notice that $\mathrm{mod}(\cdot,\cdot)$ stands for the modulus operation and $\lfloor\cdot\rfloor$ denotes the floor operation for a real number.

It is worth noting that we define $\zeta_{n,l} = \arg[\boldsymbol{a}_{\mathrm{r,i}}\left(\varphi_{n,l}, \vartheta_{n,l}\right)]$ and $\zeta_{m,l} = \arg[\boldsymbol{a}_{\mathrm{i,t}}\left(\varphi_{m,l}, \vartheta_{m,l}\right)]$, where $\arg[\cdot]$ represents the phase of a complex number. With a large-scale antenna array, the formed beam is narrow and paths are assumed to be orthogonal [10]. Thus, we assume that

$$\begin{aligned}\boldsymbol{a}_t^{\mathrm{H}}(\theta_m)\boldsymbol{a}_t(\theta_{m'}) &\approx \delta(m-m'), \\ \boldsymbol{a}_r^{\mathrm{H}}(\theta_n)\boldsymbol{a}_r(\theta_{n'}) &\approx \delta(n-n'),\end{aligned} \tag{6}$$

where $\delta(\cdot)$ represents the Dirac delta function.

After some simple algebraic operations, (1) can be rewritten as

$$\mathbf{H} = \sum_{l=1}^{L}\sum_{n=1}^{N_{ts}}\sum_{m=1}^{M_{ts}} h_n g_m \boldsymbol{a}_r\left(\theta_n\right) e^{j(\phi_l - \zeta_{n,l} - \zeta_{m,l})} \boldsymbol{a}_t^{\mathrm{H}}\left(\theta_m\right). \tag{7}$$

We aim to identify the optimal phase shift design to specify the reflection phases at each terminal, which can be obtained by the controller through the feedback of the Tx [18], [20], i.e., $\phi_l = \zeta_{n,l} + \zeta_{m,l}$. In addition, each element of the RIS is capable of inducing an independent phase shift on the incident signals

TABLE I
PROPOSED RIS-SSM SCHEME WITH $M_s = 4, N_s = 4$, AND QPSK

$[b_1b_2b_3b_4]$	$[m,\ n]$	$[b_1b_2b_3b_4]$	$[m,\ n]$
0000	$1^{\#}$, $1^{\#}$	1000	$3^{\#}$, $1^{\#}$
0001	$1^{\#}$, $2^{\#}$	1001	$3^{\#}$, $2^{\#}$
0010	$1^{\#}$, $3^{\#}$	1010	$3^{\#}$, $3^{\#}$
0011	$1^{\#}$, $4^{\#}$	1011	$3^{\#}$, $4^{\#}$
0100	$2^{\#}$, $1^{\#}$	1100	$4^{\#}$, $1^{\#}$
0101	$2^{\#}$, $2^{\#}$	1101	$4^{\#}$, $2^{\#}$
0110	$2^{\#}$, $3^{\#}$	1110	$4^{\#}$, $3^{\#}$
0111	$2^{\#}$, $4^{\#}$	1111	$4^{\#}$, $4^{\#}$
$[b_5b_6]$	s	$[b_5b_6]$	s
00	$\frac{1+i}{\sqrt{2}}$	11	$\frac{-1-i}{\sqrt{2}}$
01	$\frac{1-i}{\sqrt{2}}$	10	$\frac{-1+i}{\sqrt{2}}$

independently [4]. After some simple algebraic operations, (7) can be equivalently expressed as

$$\mathbf{H} = L \sum_{n=1}^{N_{ts}} \sum_{m=1}^{M_{ts}} h_n g_m \boldsymbol{a}_r\left(\theta_n\right) \boldsymbol{a}_t^{\mathrm{H}}\left(\theta_m\right). \tag{8}$$

B. RIS-SSM Transmission

As can be seen from Fig. 1, the transmissions of information bits of RIS-SSM can be divided into two parts. In the Tx-RIS part, the Tx utilizes a single RF link that is connected to all transmit antennas via a phase-shifting network, which is used to transmit a beam at each transmission time. In the RIS-Rx part, according to the channel state information (CSI) associated with the selected beam, the phase shifts of RIS elements are adjusted so that an equivalent directional angle over Tx-RIS-Rx is equal to zero.

In the RIS-SSM scheme, the gain amplitudes $|g_m|$ of the M_{ts} and $|h_n|$ of the N_{ts} can be respectively sorted in descending order as follows: $|g_1| > |g_2| > \cdots > |g_{M_{ts}}|$ and $|h_1| > |h_2| > \cdots > |h_{N_{ts}}|$. M_s and N_s scatterers can be respectively selected with higher gains from M_{ts} and N_{ts} scatterers, which participate in the signal transmission and determine the beam directions of the transmitted signal from the Tx and RIS, respectively. Additionally, a size-K constellation $\mathrm{s} = [s_1, s_2, \cdots, s_K]$ with $\mathbb{E}\left[s_k s_k^*\right] = 1$ is adopted, where $k \in [1, 2, \cdots, K]$ denotes the symbol index, $\mathbb{E}[\cdot]$ is the expectation operator, and $(\cdot)^*$ represents the complex conjugate operator. Denoting $\mathbf{w}_m$ as the beamforming vector satisfying $\|\mathbf{w}_m\|^2 = 1$ towards the m-th scatterer, the received signal vector from the n-th scatterer, $\mathbf{y}(n)$, is given by

$$\mathbf{y}(n) = \sqrt{E}\mathbf{H}\mathbf{w}_m s_k + \mathbf{n}, \tag{9}$$

where E denotes the transmission power, and $\mathbf{n}$ is the complex additive white Gaussian noise (AWGN) vector following $\mathcal{CN}(\mathbf{0}, \sigma_n^2 \mathbf{I}_{N_s})$, where $\mathbf{I}_{N_s}$ denotes the $N_s \times N_s$ identity matrix.

In order to facilitate the understanding of the process of RIS-SSM, we introduce an example about M_s = 4, N_s = 4, and quadrature phase shift keying (QPSK). Besides, $(\log_2(M_s) + \log_2(N_s) + \log_2(K))$ bits per channel use (bpcu) are randomly generated. In addition, we consider that the independent sequence of information bits is denoted by $\mathbf{b} = [b_1, b_2, b_3, b_4, b_5, b_6]$. The detailed transmission information can be found in Table I. For $\mathbf{b} = [000000]$, the received signal from scatterers $n = 1$ and $m = 1$ can be expressed as

$$\mathbf{y}(1) = \sqrt{E} L h_1 g_1 \boldsymbol{a}_r\left(\theta_1\right) \left[\frac{1+i}{\sqrt{2}}\right] + \mathbf{n}. \tag{10}$$

C. RIS-SSM Detection

To identify which scatterer the received beam comes from, the Rx side should be equipped with $N_{\mathrm{RF}} > N_{\mathrm{s}}$ RF links. Every RF link is connected to all antennas through a phase-shifting network, which has the ability to distinguish the received beam direction. Note that for uplink communications, this will be promising as a Rx architecture for SSM. As such, the beams from N_{s} scatterers can be distinguished simultaneously at the Rx side. The detected signal after the RF chain can be described as

$$\mathbf{y}_{\mathrm{RF}}(n_e) = \left[\boldsymbol{a}_{\mathrm{r}}^{\mathrm{H}}\left(\theta_1\right), \cdots, \boldsymbol{a}_{\mathrm{r}}^{\mathrm{H}}\left(\theta_{n_e}\right), \cdots, \boldsymbol{a}_{\mathrm{r}}^{\mathrm{H}}\left(\theta_{N_s}\right)\right] \mathbf{y}(n), \tag{11}$$

where $\mathbf{y}_{\mathrm{RF}}(n_e)$ denotes the detection signal after the RF chain, and $\boldsymbol{a}_{\mathrm{r}}^{\mathrm{H}}\left(\theta_{n_e}\right)$, $n_e \in \{1, \cdots, N_s\}$, denotes the phase shifter weight towards to the scatterer n_e. After some algebraic operations, we can evaluate (11) as follows:

$$\mathbf{y}_{\mathrm{RF}}(n_e) = \mathbf{u}_{n,m,k}(n_e) + \mathbf{n}_{\mathrm{RF}}, \tag{12}$$

where $\mathbf{u}_{n,m,k}(n_e) = \delta\left(n_e - n\right)\sqrt{E} L h_n g_m s_k$, and $\mathbf{n}_{\mathrm{RF}} = \boldsymbol{a}_{\mathrm{r}}^{\mathrm{H}}\left(\theta_{n_e}\right)\mathbf{n}$ follows $\mathcal{CN}(\mathbf{0}, \sigma_n^2 \mathbf{I}_{N_s})$ distribution. The detector employs a maximum likelihood (ML) detector, which can be expressed as

$$\left[\hat{m}, \hat{n}, \hat{k}\right] = \underset{\substack{m \in \{1,\ldots,M_s\} \\ n \in \{1,\ldots,N_s\} \\ k \in \{1,\ldots,K\}}}{\arg\min} \left\|\mathbf{y}_{\mathrm{RF}}\left(n_e\right) - \mathbf{u}_{n,m,k}(n_e)\right\|_{\mathrm{F}}^2, \tag{13}$$

where $\|\cdot\|_{\mathrm{F}}$ denotes Frobenius norm. Note that a specfic scatterer and a constellation symbol are jointly detected.

III. PERFORMANCE ANALYSIS

In this section, analytical derivation is investigated for the calculation of the theoretical upper bound on the BER of the proposed RIS-SSM scheme. The true transmission directions and transmitted symbol are denoted by m, n, and k, while $\hat{m}$, $\hat{n}$, and $\hat{k}$ denote the corresponding decoded signals after the ML detector.

A. CPEP with $\hat{n} = n$

In this case, the detection error comes from the scatterer $\hat{m}$ and signal domain information $s_{\hat{k}}$. Hence, the CPEP can be

given as

$$\begin{aligned}
&P_r\left([m,n,k]\to[\hat{m},\hat{n},\hat{k}]\mid h_1,\cdots,h_{N_s},g_1,\cdots,g_{M_s}\right)\\
=&P_r\left(\|\mathbf{y}_{\mathrm{RF}}(n_e)-\mathbf{u}_{n,m,k}(n_e)\|_{\mathrm{F}}^2>\left\|\mathbf{y}_{\mathrm{RF}}(n_e)-\mathbf{u}_{\hat{n},\hat{m},\hat{k}}(n_e)\right\|_{\mathrm{F}}^2\right)\\
=&P_r\left(\|\mathbf{n}_{\mathrm{RF}}\|_{\mathrm{F}}^2>\left\|\mathbf{n}_{\mathrm{RF}}+\mathbf{u}_{n,m,k}(n_e)-\mathbf{u}_{n,\hat{m},\hat{k}}(n_e)\right\|_{\mathrm{F}}^2\right)\\
\overset{(a)}{=}&P_r\left(\|\mathbf{n}_{\mathrm{RF}}\|_{\mathrm{F}}^2>\left\|\mathbf{n}_{\mathrm{RF}}+\sqrt{E}Lh_n\left(g_ms_k-g_{\hat{m}}s_{\hat{k}}\right)\right\|_{\mathrm{F}}^2\right)\\
=&P_r\left(-|\sqrt{E}Lh_n\left(g_ms_k-g_{\hat{m}}s_{\hat{k}}\right)|^2\right.\\
&\left.-2\Re\left\{\mathbf{n}_{\mathrm{RF}}\sqrt{E}Lh_n\left(g_ms_k-g_{\hat{m}}s_{\hat{k}}\right)\right\}>0\right)\\
=&P_r(G>0),
\end{aligned}\tag{14}$$

where $\Re\{\cdot\}$ is the real part of a complex variable. Let $G\sim\mathcal{N}\left(\mu_G,\sigma_G^2\right)$, $\mu_G=-|\sqrt{E}Lh_n\left(g_ms_k-g_{\hat{m}}s_{\hat{k}}\right)|^2$, and $\sigma_G^2=2\sigma_n^2|\sqrt{E}Lh_n\left(g_ms_k-g_{\hat{m}}s_{\hat{k}}\right)|^2$. Note that (a) is obtained by applying (12). Then, (14) can be evaluated as

$$\begin{aligned}
&P_r\left([m,n,k]\to[\hat{m},\hat{n},\hat{k}]\mid h_1,\cdots,h_{N_s},g_1,\cdots,g_{M_s}\right)\\
&=Q\left(\sqrt{\mu_G^2/\sigma_G^2}\right)=Q\left(\sqrt{0.5\rho\left|Lh_n\right|^2\left|g_ms_k-g_{\hat{m}}s_{\hat{k}}\right|^2}\right),
\end{aligned}\tag{15}$$

where $Q(\cdot)$ is the Q-function, and $\rho=E/\sigma_n^2$ denotes average SNR.

B. CPEP with $\hat{n}\neq n$

When $\hat{n}\neq n$, detection of transmission direction from the RIS is incorrect.

$$\begin{aligned}
&P_r\left([m,n,k]\to[\hat{m},\hat{n},\hat{k}]\mid h_1,\cdots,h_{N_s},g_1,\cdots,g_{M_s}\right)\\
\overset{(a)}{=}&P_r\left(\|\mathbf{y}_{\mathrm{RF}}(n_e)-\mathbf{u}_{n,m,k}(n_e)\|_{\mathrm{F}}^2>\left\|\mathbf{y}_{\mathrm{RF}}(n_e)-\mathbf{u}_{\hat{n},\hat{m},\hat{k}}(n_e)\right\|_{\mathrm{F}}^2\right)\\
=&P_r\left(\|\mathbf{n}_{\mathrm{RF}}\|_{\mathrm{F}}^2>\left\|\mathbf{n}_{\mathrm{RF}}+\mathbf{u}_{n,m,k}(n_e)-\mathbf{u}_{\hat{n},\hat{m},\hat{k}}(n_e)\right\|_{\mathrm{F}}^2\right).
\end{aligned}\tag{16}$$

Then, we have

$$\mathbf{u}_{n,m,k}(n_e)-\mathbf{u}_{\hat{n},\hat{m},\hat{k}}(n_e)=\begin{cases}\sqrt{E}Lh_ng_ms_k, & n_e=n\\ -\sqrt{E}Lh_{\hat{n}}g_{\hat{m}}s_{\hat{k}}, & n_e=\hat{n}\\ 0, & \text{others.}\end{cases}\tag{17}$$

Similar to the derivation of (14) and (15), (16) can be expressed as

$$\begin{aligned}
&P_r\left([m,n,k]\to[\hat{m},\hat{n},\hat{k}]\mid h_1,\cdots,h_{N_s},g_1,\cdots,g_{M_s}\right)\\
&=Q\left(\sqrt{0.5\rho L^2\left(\left|h_{\hat{n}}g_{\hat{m}}s_{\hat{k}}\right|^2+\left|h_ng_ms_k\right|^2\right)}\right).
\end{aligned}\tag{18}$$

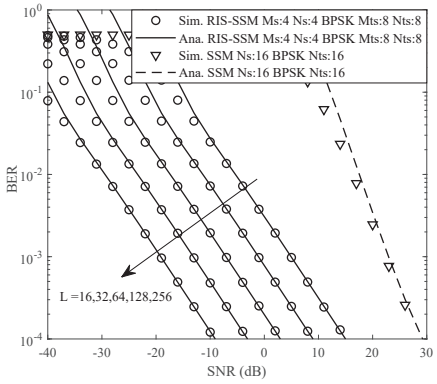

Fig. 2. BER of the RIS-SSM systems and comparison with that of the SSM system.

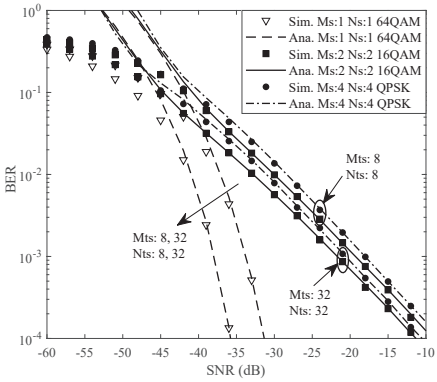

Fig. 3. Tradeoff between M_s = N_s and K for the RIS-SSM system with L = 256 in the cases of $M_{ts}=N_{ts}$ = 8 and 32, respectively.

Therefore, the CPEP can be described as

$$\begin{aligned}
&P_r\left([m,n,k]\to[\hat{m},\hat{n},\hat{k}]\mid h_1,\cdots,h_{N_s},g_1,\cdots,g_{M_s}\right)\\
&=\begin{cases}Q\left(\sqrt{0.5\rho\left|Lh_n\right|^2\left|g_ms_k-g_{\hat{m}}s_{\hat{k}}\right|^2}\right), & n_e=n\\ Q\left(\sqrt{0.5\rho L^2\left(\left|h_{\hat{n}}g_{\hat{m}}s_{\hat{k}}\right|^2+\left|h_ng_ms_k\right|^2\right)}\right), & n_e\neq n.\end{cases}
\end{aligned}\tag{19}$$

C. Union bound on the BER

On the basis of (19), an analytical upper bound on the BER of the RIS-SSM scheme can be evaluated by (20) [10], [13], [14], shown at the bottom of this page. In (20), $P\left([m,n,k]\to[\hat{m},\hat{n},\hat{k}]\mid h_1,\cdots,h_{N_s},g_1,\cdots,g_{M_s}\right)$ denotes the CPEP, and $N\left([m,n,k]\to[\hat{m},\hat{n},\hat{k}]\right)$ represents the Hamming distance between $[m,n,k]$ and $[\hat{m},\hat{n},\hat{k}]$.

IV. Numerical Results

In this section, the BER of the proposed RIS-SSM scheme presents the analytical curves and simulation results for various

$$\mathrm{BER}\leq\sum_{m=1}^{M_\mathrm{s}}\sum_{n=1}^{N_\mathrm{s}}\sum_{k=1}^{K}\sum_{\hat{m}=1}^{M_\mathrm{s}}\sum_{\hat{n}=1}^{N_\mathrm{s}}\sum_{\hat{k}=1}^{K}\frac{N\left([m,n,k]\to[\hat{m},\hat{n},\hat{k}]\right)P_r\left([m,n,k]\to[\hat{m},\hat{n},\hat{k}]\mid h_1,\cdots,h_{N_s},g_1,\cdots,g_{M_s}\right)}{M_sN_sK\log_2(M_\mathrm{s}N_\mathrm{s}K)}.\tag{20}$$

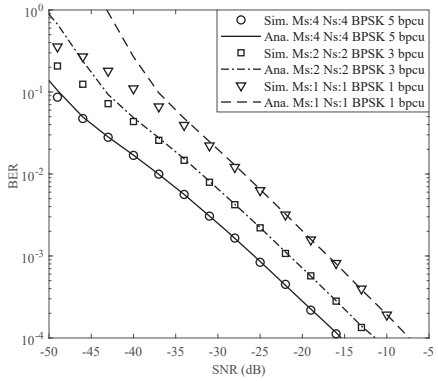

Fig. 4. BER for various data rates of RIS-SSM systems with $M_{ts} = N_{ts} = 16$ and $L = 256$.

scenarios. Particularly, simulation results are used to check the correctness of the analytical curves. In addition, we assume $d_{\mathrm{r}} = d_{\mathrm{t}} = d_{\mathrm{x}} = d_{\mathrm{y}} = \lambda/2$. Also, the non-line-of-sight scenario is considered in the dual-hop communication paths. It is worth noting that signal domain k is considered *K*-ary phase shift keying/quadrature amplitude modulation (PSK/QAM).

In Fig. 2, the BER of the proposed RIS-SSM system as a function of L is compared with that of the conventional SSM, in which the desired signal is transmitted from the Tx through a target scatterer to the Rx without RIS. As seen from Fig. 2, the higher the number of reflecting elements of the RIS, the more obvious the superiority of the scheme becomes. Additionally, the BER of the RIS-SSM system extremely outperforms the conventional SSM system even in the low SNR region. Thus, the proposed RIS-SSM system can achieve high level of successfully transmissions over the considered SNR ranges.

Fig. 3 indicates the BER performance of the trade-off between the scattering domain $M_s = N_s$ and signal domain K for RIS-SSM systems at a different total number of scatterers. As clearly seen from this figure, the BER of the proposed RIS-SSM scheme can be improved by increasing the M_{ts} and N_{ts} values from 8 to 32, respectively. In addition, the BER of the RIS-SSM system with $M_s = N_s = 2$ and 16QAM is slightly better than that of the RIS-SSM system with $M_s = N_s = 4$ and QPSK. It is worth noting that the BER of the RIS-SSM with $M_s = N_s = 1$ and 64QAM is significantly superior to the previous two configurations.

The BER of RIS-SSM systems versus SNR for different values of bpcu is depicted in Fig. 4. It should be noticed that a successful information transmission demands high SNR values. By comparing 1, 3, and 5 bpcu, we observe that the RIS-SSM can provide more reliable communications with a lower data rate. As the modulation order is higher, the Euclidean distance between the constellation points is reduced after signal normalization, which leads to the greater the probability of misjudgment.

V. Conclusions and Future Works

A novel RIS-SSM scheme has been proposed to enhance the reliability of signal transmission over wireless channels. The ML detector has been developed and a closed-form upper bound on the BER under Saleh-Valenzuela channel has been derived. Moreover, Monte Carlo simulation results have demonstrated that the accuracy of the theoretic analysis and demonstrated that the proposed RIS-SSM system outperforms the traditional SSM system in terms of the BER. Our future work will concentrate on how CSI is obtained, and evaluating the performance of the proposed RIS-SSM under the imperfect CSI. Designing a practical phase-shift model for this scheme, which captures the phase-dependent amplitude variations, appears as an interesting and open research topic, which will also be considered in our future work.

References

[1] C. Pan *et al.*, "Reconfigurable intelligent surfaces for 6G systems: Principles, applications, and research directions," *IEEE Commun. Mag.*, vol. 59, no. 6, pp. 14-20, Jun. 2021.

[2] W. Saad, *et al.*, "A vision of 6G wireless systems: Applications, trends, technologies, and open research problems," *IEEE Netw.*, vol. 34, no. 3, pp. 134-142, May/Jun. 2020.

[3] S. Dang, *et al.*, "What should 6G be?" *Nat. Electron.*, vol. 3, no. 1, pp. 20-29, Jan. 2020.

[4] Q. Wu, *et al.*, "Intelligent reflecting surface aided wireless communications: A tutorial," *IEEE Trans. Commun.*, vol. 69, no. 5, pp. 3313-3351, May 2021.

[5] Q. Wu and R. Zhang, "Intelligent reflecting surface enhanced wireless network via joint active and passive beamforming," *IEEE Trans. Wireless Commun.*, vol. 18, no. 11, pp. 5394-5409, Nov. 2019.

[6] S. Sun, *et al.*, "MIMO for millimeter-wave wireless communications: Beamforming, spatial multiplexing, or both?" *IEEE Commun. Mag.*, vol. 52, no. 12, pp. 101-121, Dec. 2014.

[7] W. Tan, *et al.*, "Analysis of different planar antenna arrays for mmWave massive MIMO systems," in *Proc. IEEE 85th Veh. Technol. Conf. (VTC Spring)*, Sydney, NSW, Australia, Jun. 2017, pp. 1-5.

[8] M. D. Renzo, *et al.*, "Reconfigurable intelligent surfaces vs. relaying: Differences, similarities, and performance comparison," *IEEE Open J. of the Commun. Society*, vol. 1, pp. 798-807, Jun. 2020.

[9] E. Basar, *et al.*, "Wireless communications through reconfigurable intelligent surfaces," *IEEE Access*, vol. 7, pp. 116753-116773, Aug. 2019.

[10] Y. Ding, *et al.*, "Spatial scattering modulation for uplink millimeter-wave systems," *IEEE Commun. Lett.*, vol. 21, no. 7, pp. 1493-1496, Jul. 2017.

[11] J. Zhang, *et al.*, "Adaptive spatial scattering modulation," *IEEE Trans. Wireless Commun.*, vol. 20, no. 10, pp. 6680-6690, Oct. 2021.

[12] Y. Tu, *et al.*, "Generalized spatial scattering modulation for uplink millimeter wave MIMO system," in *2018 IEEE/CIC Int. Conf. Commun. in China (ICCC)*, Aug. 2018, pp. 22-27.

[13] S. Ruan, *et al.*, "Diversity analysis for spatial scattering modulation in millimeter wave MIMO system," in *2019 11th Int. Conf. on Wireless Commun. and Signal Process. (WCSP)*, Sep. 2019, pp. 1-5.

[14] Q. Li, *et al.*, "Polarized spatial scattering modulation," *IEEE Commun. Lett.*, vol. 23, no. 12, pp. 2252-2256, Dec. 2019.

[15] E. Basar, "Reconfigurable intelligent surface-based index modulation: A new beyond MIMO paradigm for 6G," *IEEE Trans. Commun.*, vol. 68, no. 5, pp. 3187-3196, May 2020.

[16] W. Yan, X. Yuan and X. Kuai, "Passive beamforming and information transfer via large intelligent surface," *IEEE Wireless Commun. Lett.*, vol. 9, no. 4, pp. 533-537, Apr. 2020.

[17] T. Ma, *et al.*, "Large intelligent surface assisted wireless communications with spatial modulation and antenna selection," *IEEE J. Sel. Areas Commun.*, vol. 38, no. 11, pp. 2562-2574, Nov. 2020.

[18] C. Huang, *et al.*, "Reconfigurable intelligent surfaces for energy efficiency in wireless communication," *IEEE Trans. Wireless Commun.*, vol. 18, no. 8, pp. 4157-4170, Aug. 2019.

[19] Q. Li, *et al.*, "Space shift keying with reconfigurable intelligent surfaces: Phase configuration designs and performance analysis," *IEEE Open J. Commun. Soc.*, vol. 2, pp. 322-333, Feb. 2021.

[20] B. C. Nguyen, *et al.*, "On performance of two-way full-duplex communication system with reconfigurable intelligent surface," *IEEE Access*, vol. 9, pp. 81274-81285, Jun. 2021.